

# Mechanism of Spiral Wave Unpinning in the Belousov–Zhabotinsky Reaction with a DC Electric Field

S. V. Amrutha, Anupama Sebastian, Puthiyapurayil Sibeesh, Shreyas Punacha, and T. K. Shajahan\*



Cite This: *J. Phys. Chem. C* 2022, 126, 19618–19626



Read Online

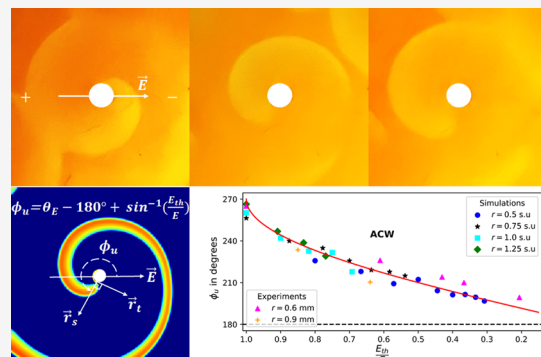
ACCESS |

Metrics & More

Article Recommendations

Supporting Information

**ABSTRACT:** We study the mechanism of spiral wave unpinning in the Belousov–Zhabotinsky (BZ) reaction with a DC electric field. The unpinning is characterized by the phase of the spiral tip around the obstacle boundary at the time of unpinning. We systematically measure the unpinning phase as a function of the chirality of spiral rotation, the initial phase of the spiral, the size of the pinning obstacle, the direction, and the strength of the applied electric field. In both BZ experiments and simulations using the Oregonator model, we observe that the spiral wave always unpins at a fixed position with respect to the applied field. The wave unpins when the electric field component in the direction of the tip velocity of the spiral waves becomes equal to a threshold field strength. From these observations, we deduce a relation between the phase of unpinning, the size of the pinning obstacle, the strength, and the direction of the electric field, and it agrees with our observations. We conclude from our observations that a retarding ‘electric force’ on the chemical wave is responsible for the unpinning in the BZ medium. Our results indicate that the ‘electric force’ is more effective in unpinning when the wave moves away from the anode than when it is moving toward it.



## INTRODUCTION

A wide variety of physical, chemical, and biological systems display traveling wave patterns where an excitation characteristic to the substrate propagates as a wave. Examples include chemical waves in the Belousov–Zhabotinsky (BZ) reaction,<sup>1</sup> waves of cellular action potential in cardiac tissue,<sup>2</sup> CO oxidization wave on a metal surface,<sup>3</sup> corrosion waves on steel in nitric acid,<sup>4</sup> cellular signaling waves in the social amoeba *Dictyostelium discoideum*,<sup>5</sup> and oscillating proteins on the surface of *Xenopus* frog embryos.<sup>6</sup> These different types of systems are collectively called excitable media. They all have a characteristic response to an external stimulus, provided the stimulus is above a threshold, and afterward, they do not respond to another stimulus for a fixed time period. These excitations can form traveling waves, like concentric circles from the point of stimulus<sup>7</sup> or self-sustained rotating spiral waves.<sup>8</sup>

All excitation waves, irrespective of the mechanism of formation and the nature of the substrate medium, have very similar dynamics. The spiral waves can get attracted to heterogeneities in the medium and form very stable rotating patterns around the boundary of these heterogeneities.<sup>9–11</sup> Such pinning has been observed in chemical systems and also in physiological tissue, both in the experimental settings and in their mathematical models.<sup>12–14</sup> The pinned waves are very stable, and they can only be unpinned by careful external intervention.<sup>15–17</sup> This problem has attracted attention

recently because such pinned waves are believed to play an essential role in cardiac arrhythmia control.<sup>18</sup>

The mechanism of unpinning is very different for the pinned waves in the BZ reaction as opposed to such waves in the cardiac tissue. Because the chemical waves in the BZ reaction are constituted of charged ions, they can directly interact with an external electric field.<sup>19–21</sup> Unpinning in the physiological system is possible with carefully delivered secondary excitation generated by the electric field, which is absent in the chemical medium.<sup>22–24</sup> In this paper, we investigate the field-induced unpinning of chemical waves.

Theoretical studies on the analysis of chemical wave propagation have suggested that an applied field may significantly alter wave propagation.<sup>21,25</sup> A DC electric field in the BZ reaction can alter the wave velocity, and it can also cause annihilation and splitting of the waves.<sup>26,27</sup> The spiral wave is forced to drift in the direction of the anode but with a perpendicular velocity component whose direction is determined by the chirality of the spiral.<sup>19,28,29</sup> The spiral can be dragged in this fashion and ultimately removed from the

Received: March 1, 2022

Revised: October 28, 2022

Published: November 14, 2022



medium. An electric field can unpin a pinned spiral wave if the applied current is above a threshold current density.<sup>30</sup> This threshold increases linearly with the radius of the pinning heterogeneity.<sup>31</sup> A study in a three-dimensional BZ system demonstrated that pinned scroll waves also could be unpinned by external electric fields.<sup>32</sup> However, the mechanism of field-induced unpinning is not addressed so far. Apart from DC electric field, many groups also have studied the response of free spirals to AC and polarized electric fields.<sup>21</sup> A corotating circularly polarized electric field (CPEF) provides maximum spiral drift,<sup>21,33</sup> and it can induce frequency synchronization of the spiral with the applied CPEF.<sup>34</sup> It has been shown that the chirality of the spiral can be controlled by adjusting the frequency of the CPEF.<sup>35</sup> Experiments in the BZ reaction have shown that spiral turbulence can be successfully controlled with CPEF.<sup>36</sup>

To understand the unpinning of chemical waves in an electric field, we need to study how the pinned wave leaves heterogeneity. This article reports a detailed investigation of the location at which the spiral wave leaves the pinning obstacle in the BZ reaction as a function of the chirality of spiral rotation, the initial phase of the spiral, the size of the pinning obstacle, direction, and the strength of the applied electric field. We study unpinning both in the experiments and numerical simulations of the Oregonator model. From the observations, we deduce a relationship between the phase of unpinning, the size of the pinning obstacle, the strength, and the direction of the electric field.

## METHODS

**Experimental Methods.** We performed experiments in uniform thin layers of the ferroin-catalyzed Belousov–Zhabotinsky (BZ) reaction. The reaction mixture is embedded in a 1.4%w/v agar gel to avoid any hydrodynamic perturbations if present.<sup>37</sup> First, the agar powder is dissolved in deionized water, and then the reagents—sulfuric acid, sodium bromate, malonic acid, and ferroin—are added sequentially into the mixture. The initial concentrations of reagents in the medium are  $[H_2SO_4] = 0.16\text{ M}$ ,  $[NaBrO_3] = 40\text{ mM}$ , [malonic acid] = 40 mM, and [ferroin] = 0.5 mM. This solution displays color oscillation between red and blue, indicating two different oxidation states of the catalyst ferroin. After one cycle of color oscillation, the mixture is poured into a glass Petri dish of diameter 10 cm. The immobilized reaction mixture has a thickness of about 3 mm. A silver wire is used to initiate an oxidation wave at the surface of the reaction medium. A pair of counter-rotating spirals is created by breaking the central induced circular wavefront with the tip of a needle.

Glass beads of different diameters are used as the pinning heterogeneity. The bead is inserted partially across the gel surface by gently pushing it into the agar gel so that the spiral tip on the surface pins to the great circle of the spherical bead. Pinning of the spiral tip to the glass bead is confirmed after two to three complete spiral rotations. A pinned spiral wave takes 4.17 min to complete a rotation around a bead of a radius of 0.6 mm in the absence of an applied electric field. The time period for the spiral pinned to obstacles of radii  $r = 0.75$  and 0.9 mm is 4.58 and 5.04 min, respectively. The error in the time measurements is 0.5 s. The rotation period increases with the size of the pinning obstacle, as reported earlier.<sup>10</sup> A schematic diagram of the experimental setup is shown in Figure 1. Unpinning experiments are performed in the

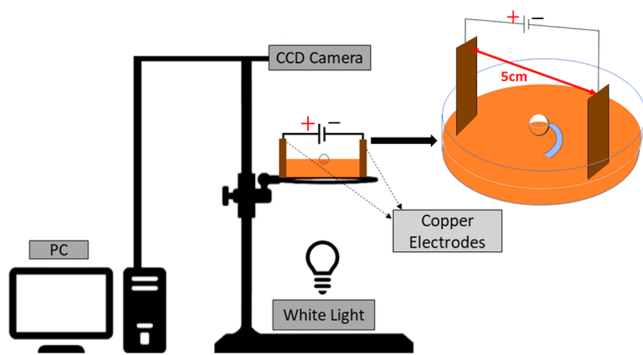


**Figure 1.** Schematic representation of the experimental setup: Images of the BZ reaction are recorded with a CCD camera controlled by LabVIEW software. The system is illuminated from the bottom with white light. Electrode positions in the medium with respect to the obstacle are illustrated in the inset. The white circle at the center of the reaction medium represents the pinning obstacle (not to scale).

presence of a constant DC electric field. We applied the field through a pair of copper electrodes (of dimension 5 cm × 2.5 cm × 0.25 mm each) kept 5 cm apart. Voltage signals are generated using a data acquisition device (NI USB-6343) controlled with LabVIEW scripts. To avoid the effects of Ohmic heating, we kept the reaction medium inside a square Petri dish filled with water. Images of the BZ reaction are recorded with a CCD camera (mvBlueCougarX120bC). The lens of the camera is equipped with a blue filter (MidOpt BP470-27), and the system is illuminated from the bottom with a white light (3W LED). Images are captured every half a second for 2–3 h. All experiments are performed at constant room temperature. We have developed LabVIEW programs for image and raw data acquisition. Image analysis is done with Python scripts. For comparison, we have performed experiments using a cylindrical rod (see Appendix A for details).

**Numerical Methods.** We used a three-variable Oregonator model for the simulation of the BZ reaction system. This model consists of the following equations<sup>29</sup>

$$\frac{\partial u}{\partial t} = \frac{1}{\epsilon}(qw - uw + u(1 - u)) + D_u \nabla^2 u \quad (1)$$

$$\frac{\partial v}{\partial t} = u - v + D_v \nabla^2 v + M_v(\vec{E} \cdot \nabla v) \quad (2)$$

$$\frac{\partial w}{\partial t} = \frac{1}{\epsilon'}(-qw - uw + fv) + D_w \nabla^2 w + M_w(\vec{E} \cdot \nabla w) \quad (3)$$

The variables  $u$ ,  $v$ , and  $w$  represent the rescaled, dimensionless form of concentrations of  $[HBrO_2]$ , the oxidized catalyst  $[Fe^{3+}]$ , and  $[Br^-]$ , respectively. The model parameters are  $q = 0.002$ ,  $f = 1.4$ ,  $\epsilon = 0.01$ , and  $\epsilon' = 0.0001$ . For both variables  $v$  and  $w$ , the electric field  $\vec{E}$ , applied along the  $+x$ -axis, is added as an advection term. However, the variable  $u$  is unaffected in the presence of an electric field as it corresponds to the charge-less species  $[HBrO_2]$ . We consider ion mobility,  $M_i \approx -z_i D_i$ , where  $z_i$  is the charge of the ion and  $D_i$  is its corresponding diffusion coefficient.<sup>38</sup> Henceforth, we assigned the values  $M_u = 0$ ,  $M_v = -2$ , and  $M_w = 1$  in our model, as shown in Table 1.

The computation domain is composed of  $300 \times 300$  grids of uniform size with  $dx = dy = 0.1$  spatial units (s.u.). The temporal evolution is studied using the explicit forward Euler method with a time step of  $dt = 0.0001$ . The domain and

**Table 1**

<i>i</i>	<i>z<sub>i</sub></i>	<i>D<sub>i</sub></i>	<i>M<sub>i</sub></i>
<i>u</i>	0	1	0
<i>v</i>	3	0.6	-2
<i>w</i>	-1	1.12	1

obstacle boundaries are both subjected to no-flux boundary conditions. At the center of the domain, an obstacle of radius  $r$  is created by reducing the value of  $D_u$  to 0.0001, while  $D_v$  and  $D_w$  are kept constant across the simulation domain. At the obstacle border, the phase-field approach is employed to set no-flux boundary conditions. We used obstacle radii ranging from 0.75 to 1.5 s.u. In each trial, we initiate the electric field at 18 different initial phases of the spiral tip that are symmetrically distributed around the obstacle. Whenever the spiral tip unpins from the obstacle, we estimate the associated detachment position.

We also have added the simulation results of the two-variable Oregonator model (the dimensionless Tyson–Fife reduction of the three-variable Oregonator model)<sup>39–41</sup> in Appendix B.

## RESULTS AND DISCUSSION

Previous studies have shown that the propagation of a chemical excitation wave can be controlled with an external electric field.<sup>26,27</sup> A free rotating spiral wave in an external electric field moves from its initial position along a trajectory at an angle to the electric field. The direction of this trajectory is determined by the strength of the applied field and the chirality of the spiral.<sup>19,21,28</sup> It was also shown that the field could be used to detach a pinned spiral wave from an inexcitable obstacle in the reaction medium.<sup>30</sup> In light of these results, we investigated the mechanism of unpinning by observing the position of spiral unpinning with respect to the direction of the applied field. We used both the experimental BZ reaction and the Oregonator model to systematically study the unpinning by an external electric field.

We measured the position of the spiral tip around the obstacle boundary at the time of unpinning in degrees from the  $+x$ -axis, and it is denoted as the unpinning phase ( $\phi_u$ ) of the

spiral. Here, the applied field is oriented along the  $+x$ -axis. In experiments, the angle at which the rotating wave detaches from the glass bead is determined from the images using software GIMP.<sup>42</sup> Experimental images have a resolution of 0.07 mm/pixel, which gives us a resolution of  $6.67^\circ$  in angle measurements for a bead of a radius of 0.6 mm. In simulations, the spiral tip is defined as the intersection of two contours  $u = 1/2$  and  $F(1/2, v) = 0$ , where  $F$  is given by the reaction term in eq (8).<sup>43</sup>

We observed that the spiral tip unpins from the obstacle only when the field strength is above a threshold ( $E_{th}$ ). We determined  $E_{th}$  by systematically ramping up the field strength to find the minimum field required to get the wave unpinned within one rotation of the spiral. Figure 2 shows the unpinning of anticlockwise (ACW) and clockwise (CW) rotating pinned spirals subjected to a uniform DC electric field of strength greater than  $E_{th}$ . It was found that both ACW and CW spirals detach near the anode as the tip propagates away from the anode. For an electric field applied along the  $+x$ -axis (i.e., for the anode situated at  $180^\circ$ ) in Figure 2, the CW spiral detached around  $135^\circ$ , and the ACW spiral detached around  $225^\circ$ . After unpinning, the tip drifts at an angle from the direction of the anode as the free spiral drifts in an electric field.<sup>19,28,29</sup>

According to Sutthiopad et al., the critical threshold ( $E_{th}$ ) increases with the size of the pinning obstacle.<sup>30</sup> We determined the  $E_{th}$  for obstacles with radii  $r = 0.6, 0.75$ , and  $0.9$  mm in experiments (Figure 3a). In terms of the spiral wavelength ( $\lambda = 3.696$  mm), these radii are  $0.162, 0.202$ , and  $0.243 \lambda$  respectively. In simulations, the obstacle radii are  $r = 0.75$  s.u ( $0.0745 \lambda$ ),  $1.0$  s.u ( $0.0994 \lambda$ ),  $1.25$  s.u ( $0.1243 \lambda$ ), and  $1.5$  s.u ( $0.149 \lambda$ ). From Figure 3b–d, it is clear that at  $E = E_{th}$ , the unpinning phase of spirals with similar chirality is constant irrespective of the obstacle size.

To find the factors influencing the unpinning phase, we applied the electric field at different initial phases of the spiral. The initial phase of a spiral,  $\phi_0$ , is the phase of the spiral tip on the obstacle boundary at the time of field initiation. For different  $\phi_0$ , the spiral unpins with a constant  $\phi_u$ , except when  $\phi_0$  is close to the expected unpinning phase itself. In such situations, the wave is unpinned with a fixed delay (Figure 4).

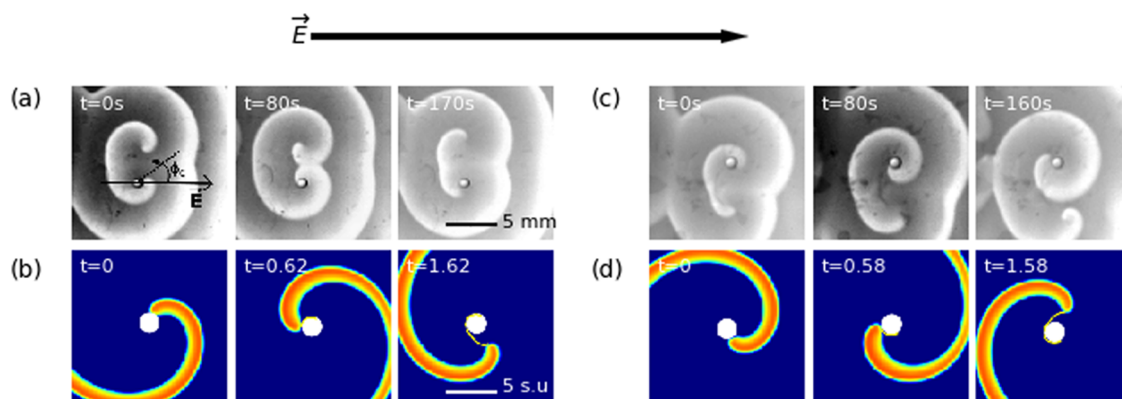


**Figure 2.** Unpinning of the spiral wave with the DC electric field: An anticlockwise (ACW) rotating spiral (a) in the experiment with initial phase  $\phi_0 = 45^\circ$  unpinned at  $\phi_u = 203.6^\circ$  and (b) in simulation with initial phase  $\phi_0 = 60^\circ$  unpinned at  $\phi_u = 236.47^\circ$ . A clockwise rotating (CW) spiral (c) in experiments with initial phase  $\phi_0 = 315^\circ$  unpinned at  $\phi_u = 151.43^\circ$  and (d) in simulations with initial phase  $\phi_0 = 300^\circ$  unpinned at  $\phi_u = 122.73^\circ$ . The field strength in the experiment is  $E = 2.40$  V/cm, and in simulation,  $E = 1.1$ . The obstacle radius in the experiment is 0.6 mm, and in simulation, it is 1.0 s.u. The bold black arrow represents the field direction. The yellow lines in (b) and (d) indicate the trajectory of the spiral tip (see Supporting Information videos).

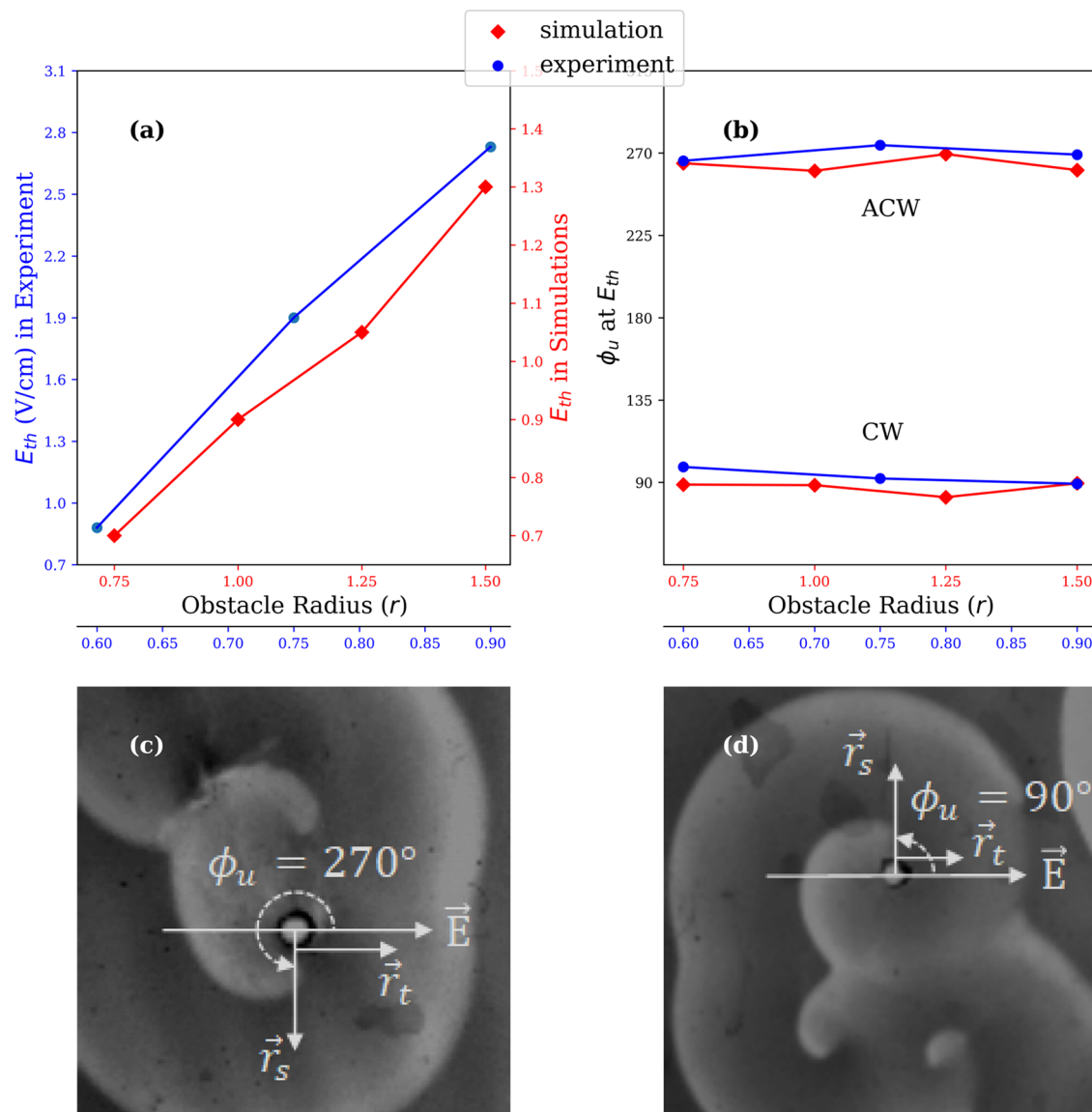


**Figure 3.** Unpinning of the spiral wave as a function of the radius of the obstacle: Threshold field strength ( $E_{th}$ ) for unpinning the spiral from obstacles having different radii is plotted. (a) In both experiments (blue dots) and simulations (red diamonds), the critical threshold for unpinning increases linearly with the obstacle size. Blue axis labels correspond to experimental data and red axis labels correspond to simulation data. The radius is measured in millimeters (mm) in experiments (lower  $+x$ -axis) and space units (s.u) in simulations (upper  $+x$ -axis). (b)  $\phi_u$  is plotted against the obstacle radius. At  $E = E_{th}$ , (c) ACW spiral always unpins at  $270^\circ$ , while (d) CW unpins at  $90^\circ$  in experiments.  $\vec{E}$  represents the field direction and  $\vec{r}_t$  is the tangential propagation vector at  $\phi_u$ . In both (c) and (d), the obstacle radius = 0.6 mm and  $E = 0.8$  V/cm.

Another parameter that can influence the unpinning is the direction of the applied field,  $\theta_E$ . For  $\theta_E = 0^\circ$  (along the  $+x$ -direction), a CW spiral unpins in between  $90$  and  $180^\circ$ . When the field direction is reversed, *i.e.*, for  $\theta_E = 180^\circ$  (along the  $-x$ -direction), the CW spiral unpins in between  $270$  and  $360^\circ$  (Figure 5). Despite the difference in the phase values, the unpinning phase is always symmetrical to the field vector.

From these observations, we hypothesize that the unpinning happens because of the slow down in the spiral tip velocity due to the electric field. The wave unpins when the electric force opposing the tip movement is above the critical threshold. From Figure 3c, it is clear that when  $E = E_{th}$ , an ACW spiral experiences the maximum electric force opposing its tip rotation at the phase  $\phi_s = 270^\circ$ . Hence, unpinning occurs at this phase. The direction of the spiral tip velocity at each phase  $\phi_s$  around the obstacle boundary is represented by  $\hat{r}_t$  (Figure

3c,d). The orientation of  $\hat{r}_t$  is  $(\phi_s + 90^\circ)$  for the ACW spiral and  $(\phi_s - 90^\circ)$  for the CW spiral. With  $E = E_{th}$ , the wave unpins when the field vector and  $\hat{r}_t$  align parallel to each other, as shown in Figure 3c,d. For  $E$  greater than  $E_{th}$ , the wave can be unpinned when the component of the applied electric field ( $\vec{E}$ ) along  $\hat{r}_t$  becomes equal to  $E_{th}$ . Based on these considerations, we calculated the unpinning phase as

$$\phi_u = \theta_E - 180^\circ + \sin^{-1}\left(\frac{E_{th}}{E}\right) \quad (4)$$

However, when the initial phase of the spiral is close to this expected unpinning phase (*i.e.*,  $\phi_u - \Delta \leq \phi_0 \leq \phi_u + \Delta$ ), the wave unpins after a fixed delay of  $\Delta$ .

$$\phi_u = \phi_0 + \Delta \quad (5)$$

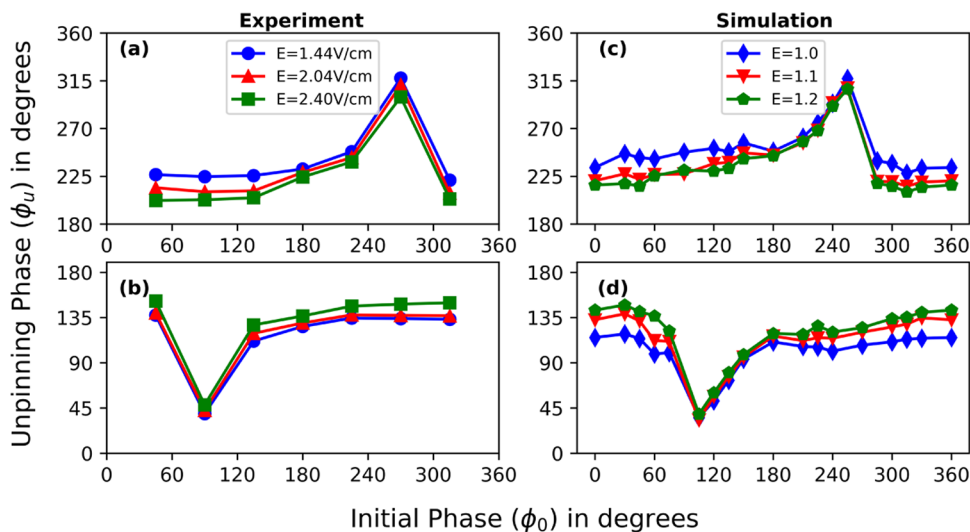


**Figure 4.** Unpinning phase as a function of the initial phase of the spiral: (a) In the experiment, the detachment phase for the ACW spiral is plotted for different initial phases.  $\phi_0$  is varied in the steps of  $45^\circ$ , for different  $E = 1.44, 2.04$ , and  $2.40 \text{ V/cm}$ .  $E_{\text{th}} = 0.8 \text{ V/cm}$  and the obstacle radius is  $0.6 \text{ mm}$ . (b) same as in (a) for CW spiral. (c) In simulations, the unpinning phase of the ACW spiral pinned to an obstacle of radius,  $r = 1.0 \text{ s.u}$  for 18 different initial phases is measured.  $\phi_u$  versus  $\phi_0$  is plotted for field strength  $E = 1.0, 1.1$ , and  $1.2$ . Here,  $E_{\text{th}} = 0.9$ . (d) same as in (c) for CW spiral in simulations.

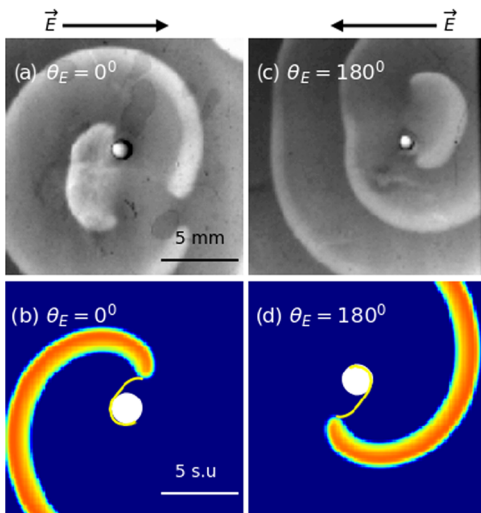


**Figure 5.** Effect of the field direction ( $\theta_E$ ) on unpinning: For  $\theta_E = 0^\circ$ , a CW spiral unpins in between  $90$  and  $180^\circ$  in (a) experiments and (b) simulations. For  $\theta_E = 180^\circ$ , a CW spiral unpins in between  $270$  and  $360^\circ$  in (c) experiments and (d) simulations. The spiral detachment position is influenced by the electric force exerted toward the anode. In experiments, obstacle radius =  $0.6 \text{ mm}$  and  $E = 2.40 \text{ V/cm}$ . In simulations, obstacle radius =  $1.0 \text{ s.u}$  and  $E = 1.1$ .

where  $\Delta = 35^\circ$  in simulation and it is about  $30^\circ$  in experiments.

Similarly, for a clockwise rotating spiral,  $\phi_u$  is

$$\phi_u = \theta_E + 180^\circ - \sin^{-1}\left(\frac{E_{\text{th}}}{E}\right) \quad (6)$$

The unpinning phases given by eq (6) are the mirror image of the unpinning phases obtained using eq (4).

At  $E = E_{\text{th}}$ , eq (6) gives  $\phi_u = 90^\circ$ , as expected from Figure 3b,d.

As with the ACW spiral, here also when the initial phase of the spiral is close to this expected unpinning angle (*i.e.*,  $\phi_u - \Delta \leq \phi_0 \leq \phi_u + \Delta$ ), then the wave unpins after a fixed delay of  $\Delta$ .

$$\phi_u = \phi_0 - \Delta \quad (7)$$

It has been observed from the study that  $E_{\text{th}}$  increases with the obstacle radius (Figure 3a). Since  $\phi_u$  depends on  $E_{\text{th}}$ ,  $\phi_u$  also increases with the obstacle radius. That is, for fixed field strength, unpinning will be delayed for a larger obstacle. Thus, the above equations relate the unpinning phase with the chirality, obstacle size, field strength, and field direction. In Figure 6, we plot  $\phi_u$  of the spiral wave as a function of  $\left(\frac{E_{\text{th}}}{E}\right)$  by varying the obstacle size and field strength for a fixed  $\theta_E$ . The maximum deviation from the predicted theoretical value is  $15^\circ$  in simulations and  $10^\circ$  in experiments. As  $\left(\frac{E_{\text{th}}}{E}\right)$  decreases,  $\phi_u$  for an ACW spiral decreases and approaches  $180^\circ$ . For spirals rotating in the CW direction, the plot between  $\phi_u$  and  $\left(\frac{E_{\text{th}}}{E}\right)$  will show the opposite trend. When  $E = E_{\text{th}}$ , the wave unpins at  $90^\circ$ . As  $E$  increases,  $\phi_u$  increases and approaches  $180^\circ$ . *i.e.*, with an increase in the field strength, unpinning happens in the close vicinity of the anode.

## CONCLUSIONS

This article reported a systematic study of the unpinning of spiral waves in a chemical excitable medium using a constant electric field. The unpinning is characterized by the unpinning phase, which is the angle of the spiral tip around the obstacle boundary at the time of unpinning. We measured the unpinning phase both in the BZ reaction medium and in the Oregonator model. It is found that for a given field strength, the spiral wave always unpins at a fixed phase while propagating away from the neighborhood of the anode. Except for a small range of initial phases, an anticlockwise (ACW) spiral unpins between  $180^\circ$  and  $270^\circ$  while a clockwise (CW) spiral unpins between  $90^\circ$  and  $180^\circ$  for an electric field applied along the  $+x$ -axis. Based on the assumption that unpinning is by the retarding force of the electric field, we estimated the unpinning phase, and it was found to be in good agreement with our measurements.

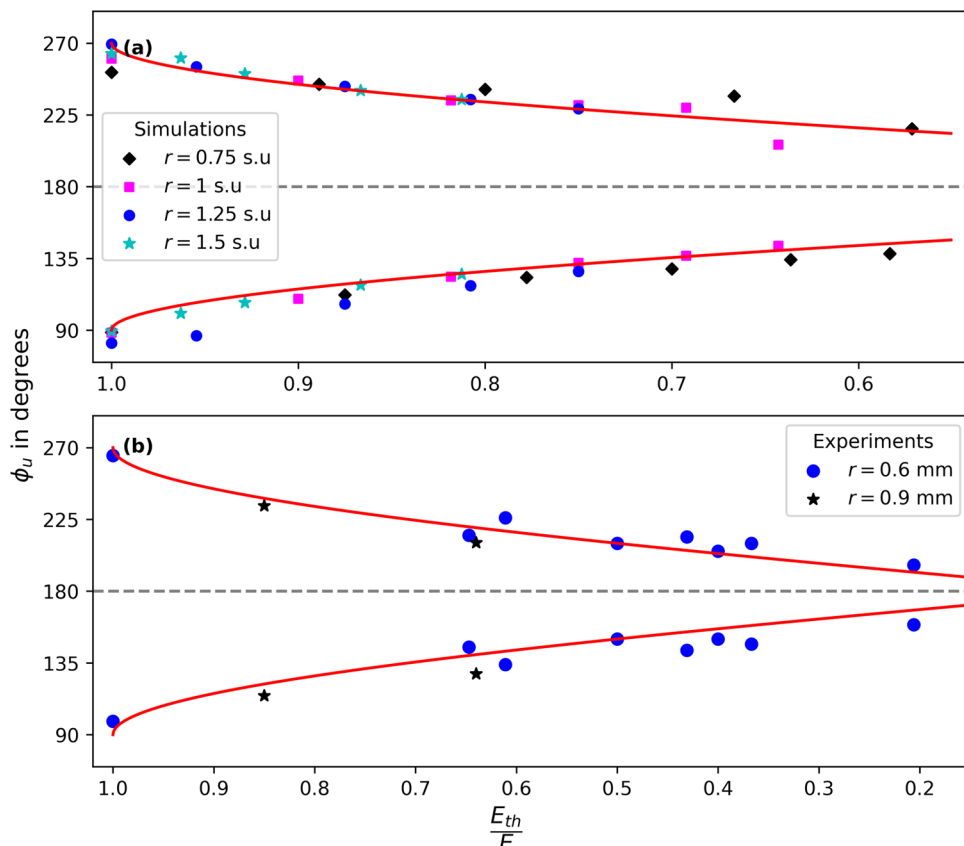


**Figure 6.** Unpinning phase varies with field strength:  $\phi_u$  is plotted against the field strength ratio  $\frac{E_{th}}{E}$  for the spiral pinned to various obstacle sizes. The radius is measured in millimeters in experiments and space units in simulations. In both (a) simulation and (b) experiment, a solid red line indicates the values of  $\phi_u$  calculated from the analytical formulae eqs (4) and (6). For both ACW and CW spirals,  $\phi_u$  approaches  $180^\circ$  with the increase in field strength. *i.e.*, an increase in the field strength results in an unpinning closer to the anode.

The observation that the wave unpins as it moves away from the anode indicates that the electric force on the chemical wave depends on the propagation direction of the wave. In particular, if the wave moves along the direction of the field, it slows down, and if the field is in the opposite direction, it accelerates. An electric field along the  $+x$ -axis accelerates an ACW spiral moving from  $0$  to  $180^\circ$  and decelerates when it moves from  $180$  to  $360^\circ$ . However, we do not observe the wave being dragged toward the anode as it approached the anode but instead slowed down as the wave moved away from it. The chemical waves in the BZ reaction involve three important chemical species: The  $\text{Br}^-$  ion,  $\text{HBrO}_2$ , and the  $\text{Fe}(\text{phen})_3^{3+}$ . The  $\text{Br}^-$  ions, usually diffuse opposite to the wave, can make the wave move slowly if the wave is moving in the same direction as the field.<sup>26</sup> Similarly, in a field opposite to the wave propagation, the  $\text{Br}^-$  ion moves ahead of the wave, leading to wave acceleration. Our results show that the slowdown effect of the field is more pronounced than its ability to accelerate the wave. Slow down in the propagation of the spiral wave when moving toward the negative electrode facilitates the unpinning of the spiral tip from the obstacle.

In the presence of an applied electric field, the core of a free spiral wave drifts toward the direction of the anode. However, the velocity of the spiral core has an additional component perpendicular to the direction of the field. The perpendicular component of the spiral drift depends on the chirality of the spiral.<sup>19</sup> Similarly, in the case of field-induced unpinning, the

position of unpinning with respect to the field changes with the chirality of spiral rotation.

The ‘electric force’ acting directly on the excitation wave is a unique feature of the chemical excitation wave. In physiological tissue, for example, though the excitation waves show very similar dynamics, the electric field does not act directly on the wavefront. For example, in cardiac tissue, the field induces secondary excitation from the boundaries of obstacles, and when they are generated within the vulnerable window of the spiral, the wave gets unpinned.<sup>22,23</sup> We have not observed such wave emission in the chemical medium; we are also not aware of any other excitable medium where the external field can directly apply a force on the excitation wave itself. In conclusion, we point out that the chemical excitation waves in the BZ reaction interact with an external electric field uniquely, and unpinning by a retarding electric force is not seen so far in any other excitable medium.

## APPENDICES

### A.. Unpinning of the Spiral Pinned to a Cylindrical Glass Rod in Experiments

We have presented the results of wave unpinning from spherical beads in the paper. Since the medium thickness is the order of the wavelength of the chemical activity, the wave patterns will be homogeneous along the third dimension. The chemical wave gets pinned around the great circle of the spherical beads—that is, along its center—most easily, and it is where the unpinning is most difficult.<sup>30</sup> We have repeated

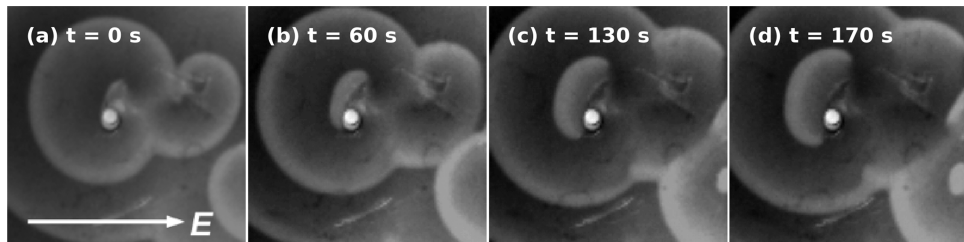


**Figure 7.** Spiral pinned to a cylindrical glass rod of a diameter of 1.0 mm is unpinned at  $\phi_u = 206.47^\circ$  with a DC electric field  $E = 2.40 \text{ V/cm}$  for  $\phi_0 = 45^\circ$ .  $E_{\text{th}} = 0.76 \text{ V/cm}$ . From the equation,  $\phi_u = 198.46^\circ$ .

these experiments using cylindrical rods to test whether the shape of the obstacles can make any difference to these results. The experimental setup is the same as in Figure 1. Instead of the glass bead, a cylindrical glass rod (length  $\approx 4 \text{ mm}$ ) is inserted vertically so that it touches the bottom of the Petri dish and stands a little high above the surface.

Figure 7 shows the unpinning of an anticlockwise (ACW) rotating spiral pinned to a cylindrical glass rod of a radius of 0.5 mm in a uniform DC electric field of strength  $E = 2.40 \text{ V/cm}$ , which is greater than the threshold ( $E_{\text{th}} = 0.76 \text{ V/cm}$ ). It was found that the spiral detaches near the anode as the tip propagates away from the anode. We measured the unpinning phase  $\phi_u = 206.47^\circ$  for an initial spiral phase  $\phi_0 = 45^\circ$ . From the equation,  $\phi_u = 198.46^\circ$ . After unpinning, the tip drifts at an angle from the direction of the anode, as in the case of a spiral pinned to a spherical glass bead.

Figure 8 shows the variation of the unpinning phase with  $\phi_0$  for a cylindrical obstacle of a radius of 1 mm. We have also

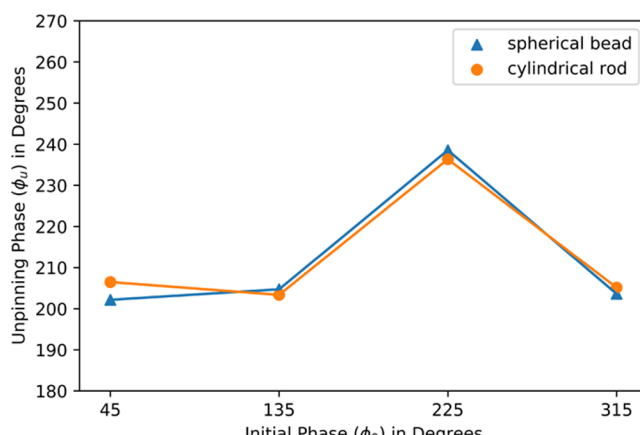


**Figure 8.** Comparison of unpinning with a spherical bead and a cylindrical rod as an obstacle: (a) Spiral pinned to a spherical glass bead of a radius of 0.6 mm is unpinned with  $E = 2.40 \text{ V/cm}$  for different spiral initial phases.  $E_{\text{th}} = 0.80 \text{ V/cm}$ . From the equation,  $\phi_u = 199.47^\circ$ . (b) Spiral pinned to a cylindrical glass rod of radius 0.5 mm is unpinned with  $E = 2.40 \text{ V/cm}$  for different spiral initial phases.  $E_{\text{th}} = 0.76 \text{ V/cm}$ . From the equation,  $\phi_u = 198.46^\circ$ .

displayed the unpinning phases corresponding to a spherical bead, and in both cases, unpinning happens at similar phases and as predicted by the theory. The unpinning threshold is slightly less for the cylindrical obstacle (0.76 V/cm) compared to the spherical bead (0.80 V/cm) because of the difference in the pinning radius. Hence, according to the analytical formula,  $\phi_u = 199.47^\circ$  for the glass bead and  $\phi_u = 198.46^\circ$  for the rod.

## B.. Simulations Using the Two-Variable Oregonator Model

In this paper, we have used a three-variable Oregonator model. All simulations of chemical waves in the BZ system have used a two-variable model. Taboada et al.<sup>44</sup> have shown that the quantitative properties of the chemical wave are the same in both the original three-variable model and the two-variable reduced model. Here, we compare the unpinning studies using both sets of model equations.

We model the BZ reaction system using a two-variable Oregonator model (the dimensionless Tyson–Fife reduction of the three-variable Oregonator model)<sup>39–41</sup> using the following equations

$$\frac{\partial u}{\partial t} = \frac{1}{\epsilon} \left( u(1-u) - \frac{fv(u-q)}{u+q} \right) + D_u \nabla^2 u + M_u (\vec{E} \cdot \nabla u) \quad (8)$$

$$\frac{\partial v}{\partial t} = u - v + D_v \nabla^2 v + M_v (\vec{E} \cdot \nabla v) \quad (9)$$

The activator variable  $u$  and the inhibitor variable  $v$  are the rescaled, dimensionless form of concentrations of  $\text{HBrO}_2$  and the catalyst, respectively. Though  $\text{HBrO}_2$  is electrically neutral, its dynamics is strongly coupled with the negatively charged  $\text{Br}^-$  ions. The effect of the electric field on the  $\text{Br}^-$  ions will be reflected immediately on the dynamics of  $\text{HBrO}_2$ .<sup>29</sup> Thus, the electric field affects both  $u$  and  $v$ , and we represent it by adding a field-induced advection term to the dynamics of both these variables. The model parameters are  $q = 0.002$ ,  $f = 1.4$ , and  $\epsilon = 0.01$  as in section “Numerical methods” in the manuscript but without the use of  $\epsilon'$ . The unidirectional electric field is  $\vec{E} = E \hat{x}$ , where  $E$  is the magnitude of the electric field. We performed simulations for both ACW and CW spirals. In the computations, we used the explicit forward Euler technique, following the same procedure as described in section “Numerical methods” of the manuscript.

In the two-variable Oregonator model, we examined the unpinning phase of the spiral pinned to an obstacle of radius  $r = 1.0 \text{ s.u}$  using an electric field of strength from  $E = 1.0, 1.1$ , and  $1.2$  and estimated the corresponding unpinning phase  $\phi_u$ . For 18 different initial phases  $\phi_0$ , around the obstacle, the unpinning phase is the same, except at the region  $\phi_0$  close to the expected  $\phi_u$  (see Figure 9). Furthermore,  $\phi_u$  reduces with the field strength. These are in good agreement with the results from the three-variable Oregonator model (see Supporting Information videos (b) and (e) for unpinning in both two- and three-variable models for the same chirality,  $E = 1.1$ ,  $r = 1.0 \text{ s.u}$ , and  $\phi_0 = 60^\circ$ ).

In two-variable, the behavior of  $\phi_u$  versus  $\sin^{-1}\left(\frac{E_{\text{th}}}{E}\right)$  curve is as predicted by our analytical formula eq (4) (see Figure 10).

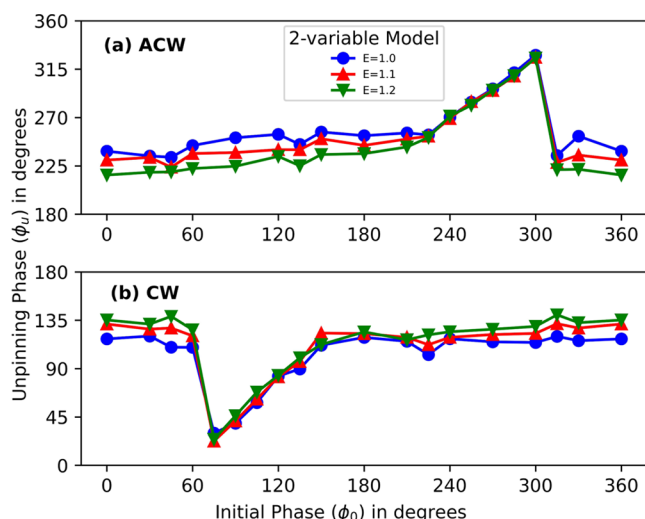


**Figure 9.** Plot of  $\phi_u$  versus  $\phi_0$  using the two-variable Oregonator model: (a) Unpinning phase of the ACW spiral pinned to an obstacle of radius,  $r = 1.0$  s.u for 18 different initial phases is measured.  $\phi_u$  versus  $\phi_0$  is plotted for field strength  $E = 1.0, 1.1$ , and  $1.2$ . Here,  $E_{\text{th}} = 0.9$ . (b) same as in (a) for the CW spiral.

The maximum deviation from the predicted theoretical value is  $7^\circ$  in simulations.

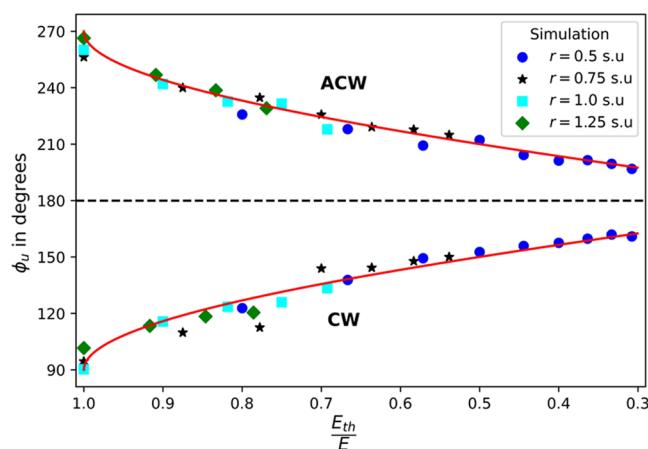


**Figure 10.** Unpinning phase with  $\frac{E_{\text{th}}}{E}$ :  $\phi_u$  obtained from the simulations using the two-variable Oregonator model is plotted against the field strength ratio  $\frac{E_{\text{th}}}{E}$  for ACW and CW spirals pinned to an obstacle of size 1.0 s.u. The solid blue line indicates the values of  $\phi_u$  calculated from the analytical formulae.

We observed an excellent agreement between the results obtained from the two- and three-variable Oregonator models. The calculated unpinning phase in both models,  $\phi_u$  matches the expected analytical formula, validating our mechanism.

## ASSOCIATED CONTENT

### Supporting Information

The Supporting Information is available free of charge at <https://pubs.acs.org/doi/10.1021/acs.jpcc.2c01452>.

Video 1 (MP4)

Video 2 (MP4)

Video 3 (MP4)

Video 4 (MP4)

Video 5 (MP4)

## AUTHOR INFORMATION

### Corresponding Author

T. K. Shahajan – Department of Physics, National Institute of Technology Karnataka, Mangalore 575025, India;  
 ORCID: [0000-0001-5551-1324](https://orcid.org/0000-0001-5551-1324); Email: [shajahan@nitk.edu.in](mailto:shajahan@nitk.edu.in)

### Authors

S. V. Amrutha – Department of Physics, National Institute of Technology Karnataka, Mangalore 575025, India;  
 ORCID: [0000-0002-6698-2436](https://orcid.org/0000-0002-6698-2436)

Anupama Sebastian – Department of Physics, National Institute of Technology Karnataka, Mangalore 575025, India; ORCID: [0000-0003-4353-2368](https://orcid.org/0000-0003-4353-2368)

Puthiyapurayil Sibeesh – Department of Physics, National Institute of Technology Karnataka, Mangalore 575025, India

Shreyas Punacha – Department of Physics, National Institute of Technology Karnataka, Mangalore 575025, India; ORCID: [0000-0002-4523-9627](https://orcid.org/0000-0002-4523-9627)

Complete contact information is available at:  
<https://pubs.acs.org/10.1021/acs.jpcc.2c01452>

### Author Contributions

S.V.A. and T.K.S. designed the study. S.V.A. performed the experiments. P.S. devised the experimental setup. S.P. designed the numerical study as well as the computational framework. A.S. performed numerical simulations. S.V.A. and A.S. analyzed the data, and developed the mechanism with help from T.K.S. A.S. and T.K.S. formulated the mechanism. S.V.A. and T.K.S. wrote the manuscript. All authors helped to edit the paper.

### Notes

The authors declare no competing financial interest.

## ACKNOWLEDGMENTS

The authors thank Beneesh P.B., Deepu Vijayasan, Ajith K.M., K.V. Gangadharan, and Muhammed Mansoor C.B. for their discussion. Experiments were conducted using a grant (ECR/2016/000983) from the Science and Engineering Research Board, Department of Science and Technology (SERB-DST), India.

## REFERENCES

- (1) Mikhailov, A. S.; Showalter, K. Control of waves, patterns and turbulence in chemical systems. *Phys. Rep.* **2006**, *425*, 79–194.
- (2) Alonso, S.; Bär, M.; Echebarria, B. Nonlinear physics of electrical wave propagation in the heart: a review. *Rep. Prog. Phys.* **2016**, *79*, No. 096601.
- (3) Sadeghi, P.; Dunphy, K.; Punckt, C.; Rotermund, H. Inversion of pattern anisotropy during CO oxidation on Pt (110) correlated with appearance of subsurface oxygen. *J. Phys. Chem. C* **2012**, *116*, 4686–4691.
- (4) Agladze, K.; Steinbock, O. Waves and vortices of rust on the surface of corroding steel. *J. Phys. Chem. A* **2000**, *104*, 9816–9819.
- (5) Sawai, S.; Thomason, P. A.; Cox, E. C. An autoregulatory circuit for long-range self-organization in Dictyostelium cell populations. *Nature* **2005**, *433*, 323–326.
- (6) Chatterjee, M.; Sain, A. Dynamic surface patterns on cells. *J. Chem. Phys.* **2022**, *156*, No. 084117.
- (7) Shah, S.; Wang, J. Sequential Waves in a Modified Belousov-Zhabotinsky Medium. *J. Phys. Chem. C* **2007**, *111*, 10639–10643.

- (8) Winfree, A. T. Spiral waves of chemical activity. *Science* **1972**, *175*, 634–636.
- (9) Sutthiopad, M.; Luengviriya, J.; Porjai, P.; Phantu, M.; Kanchanawarin, J.; Müller, S. C.; Luengviriya, C. Propagation of spiral waves pinned to circular and rectangular obstacles. *Phys. Rev. E* **2015**, *91*, No. 052912.
- (10) Lim, Z. Y.; Maskara, B.; Aguel, F.; Emokpae, R., Jr; Tung, L. Spiral wave attachment to millimeter-sized obstacles. *Circulation* **2006**, *114*, 2113–2121.
- (11) Shahajan, T. K.; Sinha, S.; Pandit, R. Spiral-wave dynamics depend sensitively on inhomogeneities in mathematical models of ventricular tissue. *Phys. Rev. E* **2007**, *75*, No. 011929.
- (12) Ke, H.; Zhang, Z.; Steinbock, O. Pinned chemical waves in the presence of Stokes flow. *J. Phys. Chem. A* **2014**, *118*, 6819–6826.
- (13) Zhang, J.; Tang, J.; Ma, J.; Luo, J. M.; Yang, X. Q. The dynamics of spiral tip adjacent to inhomogeneity in cardiac tissue. *Phys. A* **2018**, *491*, 340–346.
- (14) Majumder, R.; Zykov, V. S.; Panfilov, A. V. In silico optical control of pinned electrical vortices in an excitable biological medium. *New J. Phys.* **2020**, *22*, No. 023034.
- (15) Feng, X.; Gao, X.; Pan, D.-B.; Li, B.-W.; Zhang, H. Unpinning of rotating spiral waves in cardiac tissues by circularly polarized electric fields. *Sci. Rep.* **2014**, *4*, No. 4831.
- (16) Pan, D.-B.; Gao, X.; Feng, X.; Pan, J.-T.; Zhang, H. Removal of pinned scroll waves in cardiac tissues by electric fields in a generic model of three-dimensional excitable media. *Sci. Rep.* **2016**, *6*, No. 21876.
- (17) Punacha, S.; A, N. K.; Shahajan, T. K. Theory of unpinning of spiral waves using circularly polarized electric fields in mathematical models of excitable media. *Phys. Rev. E* **2020**, *102*, No. 032411.
- (18) Otani, N. F.; Wheeler, K.; Krinsky, V.; Luther, S. Termination of Scroll Waves by Surface Impacts. *Phys. Rev. Lett.* **2019**, *123*, No. 068102.
- (19) Agladze, K. I.; De Kepper, P. Influence of electric field on rotating spiral waves in the Belousov-Zhabotinsky reaction. *J. Phys. Chem. A* **1992**, *96*, 5239–5242.
- (20) Enderlein, J.; Kuhnert, L. Changing the dynamical behavior of nonlinear reaction diffusion systems by stochastic electric fields. *J. Phys. Chem. A* **1996**, *100*, 19642–19646.
- (21) Li, T.-C.; Gao, X.; Zheng, F.-F.; Pan, D.-B.; Zheng, B.; Zhang, H. A theory for spiral wave drift induced by ac and polarized electric fields in chemical excitable media. *Sci. Rep.* **2017**, *7*, No. 8657.
- (22) Luther, S.; Fenton, F. H.; Kornreich, B. G.; Squires, A.; Bittihn, P.; Hornung, D.; Zabel, M.; Flanders, J.; Gladuli, A.; Campoy, L.; et al. Low-energy control of electrical turbulence in the heart. *Nature* **2011**, *475*, 235–239.
- (23) Shahajan, T. K.; Berg, S.; Luther, S.; Krinsky, V.; Bittihn, P. Scanning and resetting the phase of a pinned spiral wave using periodic far field pulses. *New J. Phys.* **2016**, *18*, No. 043012.
- (24) Punacha, S.; Berg, S.; Sebastian, A.; Krinsky, V. I.; Luther, S.; Shahajan, T. Spiral wave unpinning facilitated by wave emitting sites in cardiac monolayers. *Proc. R. Soc. A* **2019**, *475*, No. 20190420.
- (25) Miyakawa, K.; Mizoguchi, M. Responses of an immobilized-catalyst Belousov-Zhabotinsky reaction system to electric fields. *J. Chem. Phys.* **1998**, *109*, 7462–7467.
- (26) Feeney, R.; Schmidt, S.; Ortoleva, P. Experiments on electric field-BZ chemical wave interactions: Annihilation and the crescent wave. *Phys. D* **1981**, *2*, 536–544.
- (27) Ševčíková, H.; Marek, M. Chemical waves in electric field. *Phys. D* **1983**, *9*, 140–156.
- (28) Steinbock, O.; Schütze, J.; Müller, S. Electric-field-induced drift and deformation of spiral waves in an excitable medium. *Phys. Rev. Lett.* **1992**, *68*, 248.
- (29) Schmidt, B.; Müller, S. C. Forced parallel drift of spiral waves in the Belousov-Zhabotinsky reaction. *Phys. Rev. E* **1997**, *55*, 4390.
- (30) Sutthiopad, M.; Luengviriya, J.; Porjai, P.; Tomapatanaget, B.; Müller, S. C.; Luengviriya, C. Unpinning of spiral waves by electrical forcing in excitable chemical media. *Phys. Rev. E* **2014**, *89*, No. 052902.
- (31) Porjai, P.; Sutthiopad, M.; Luengviriya, J.; Phantu, M.; Müller, S. C.; Luengviriya, C. Electrically forced unpinning of spiral waves from circular and rectangular obstacles. *Chem. Phys. Lett.* **2016**, *660*, 283–286.
- (32) Jiménez, Z. A.; Zhang, Z.; Steinbock, O. Electric-field-controlled unpinning of scroll waves. *Phys. Rev. E* **2013**, *88*, No. 052918.
- (33) Chen, J.-X.; Zhang, H.; Li, Y.-Q. Drift of spiral waves controlled by a polarized electric field. *J. Chem. Phys.* **2006**, *124*, No. 014505.
- (34) Chen, J.-X.; Zhang, H.; Li, Y.-Q. Synchronization of a spiral by a circularly polarized electric field in reaction-diffusion systems. *J. Chem. Phys.* **2009**, *130*, No. 124510.
- (35) Li, B.-W.; Cai, M.-C.; Zhang, H.; Panfilov, A. V.; Dierckx, H. Chiral selection and frequency response of spiral waves in reaction-diffusion systems under a chiral electric field. *J. Chem. Phys.* **2014**, *140*, No. 184901.
- (36) Ji, L.; Zhou, Y.; Li, Q.; Qiao, C.; Ouyang, Q. Experimental evidence of using a circularly polarized electric field to control spiral turbulence. *Phys. Rev. E* **2013**, *88*, No. 042919.
- (37) Jiménez, Z. A. Dynamical behavior of scroll rings in the presence of heterogeneities in the Belousov-Zhabotinsky excitable medium. Ph.D. thesis, The Florida State University, 2012.
- (38) Mosquera, J.; Gomez-Gesteira, M.; Perez-Munuzuri, V.; Munuzuri, A.; Perez-Villar, V. Electric Field Influence on Traveling Wave Propagation and Stationary Pattern Formation. *Int. J. Bifurcation Chaos* **1995**, *05*, 797–807.
- (39) Field, R. J.; Noyes, R. M. Oscillations in chemical systems. IV. Limit cycle behavior in a model of a real chemical reaction. *J. Chem. Phys.* **1974**, *60*, 1877–1884.
- (40) Tyson, J. J.; Fife, P. C. Target patterns in a realistic model of the Belousov-Zhabotinskii reaction. *J. Chem. Phys.* **1980**, *73*, 2224–2237.
- (41) Keener, J. P.; Tyson, J. J. Spiral waves in the Belousov-Zhabotinskii reaction. *Phys. D* **1986**, *21*, 307–324.
- (42) The GIMP Development Team, GIMP. <https://www.gimp.org>.
- (43) Barkley, D. A model for fast computer simulation of waves in excitable media. *Phys. D* **1991**, *49*, 61–70.
- (44) Taboada, J. J.; Muñozuri, A. P.; Pérez-Muñozuri, V.; Gómez-Gesteira, M.; Pérez-Villar, V. Spiral breakup induced by an electric current in a Belousov-Zhabotinsky medium. *Chaos* **1994**, *4*, 519–524.